

Anisotropic Magnetized Asteroseismic Waves

B. TRIPATHI ¹ AND DHRUBADITYA MITRA ²

¹*Department of Physics, University of Wisconsin–Madison, Madison, Wisconsin 53706, USA*

²*Nordita, KTH Royal Institute of Technology and Stockholm University, Hannes Alfvéns väg 12, 114 19 Stockholm, Sweden*

ABSTRACT

We solve for waves in a polytropic, stratified plasmas with a spatially varying background magnetic field that points along a horizontal x -direction, and with gravity that is directed along the vertical z -direction. Force balance determines the magnitude of the background magnetic field, $B_0^2 \sim z^{n+1}$, where n is the polytropic index. Using numerical and asymptotic methods, we deduce an explicit dispersion relation for fast pressure-driven waves: $\Omega^2 \sim K(2m+n)[1 + (1/M_A)^2(4 - 2\gamma + \cos^2\theta - 3\cos^4\theta)/4]$. Here, Ω is the frequency, K the wavenumber, θ the angle the wave-vector makes with the background magnetic field, M_A the Alfvénic Mach number, and m an integer representing the eigenstate. We discuss roles of such an explicit formula in asteroseismology.

Keywords: magnetohydrodynamics (MHD) — Sun: waves — Sun: magnetic fields — stars: waves — stars: magnetic fields

1. INTRODUCTION

The strengths of magnetic fields buried below the surface of stars are not known, though they are vital for improved understanding of the magnetic behaviour of stars. This challenge has impeded progress in understanding stellar magnetism and the evolution of magnetized stellar interiors. To estimate the magnetic field strength, linear asteroseismology is a promising technique (Aerts et al. 2010). The key idea is to calculate the dispersion relations of surface waves taking into account the presence of subsurface magnetic fields. Then inversion techniques are used, leveraging the observed power spectrum of oscillations, to infer the subsurface magnetic field. Thus, simple analytical dispersion relations are insightful, but obtaining such relations remains a challenge. This challenge also impacts the development of nonlinear asteroseismology (Guo 2020; Van Beeck et al. 2021, 2023), which requires linear dispersion relations to evaluate mode resonances. Consequently, the progress in magnetoseismology has been slow.

Observational studies report travel-time perturbations of acoustic waves to be a critical signature of strong magnetic fields in the stellar interior (Schunker et al. 2005;

Ilionidis et al. 2011). Numerical simulations of asteroseismic waves also suggest the possibility of detecting subsurface fields, before they emerge on the surface (Singh et al. 2014, 2015, 2016, 2020; Das et al. 2020; Das 2022). To bolster such findings, a thorough understanding of the impact of magnetic fields on asteroseismic waves is essential (Nye & Thomas 1976; Adam 1977; Thomas 1983; Campos 1983; Cally 2007; Campos & Marta 2015; Tripathi & Mitra 2022).

Waves in an unmagnetized polytropic atmosphere were exactly solved analytically by Lamb (1911) who derived the relation

$$\frac{\Omega^2}{2K} - \frac{(n+1)(n+1-\gamma n)K}{2\gamma^2\Omega^2} = m + \frac{n}{2}, \quad (1)$$

where Ω is the frequency, K the wavenumber, n the polytropic index, γ the adiabatic index, and m the eigenstate index, with $m = 0, 1, 2, \dots$. This advancement led to a series of newer and significant understanding of hydrodynamic waves. Under fast-wave approximation, $\Omega^2/K \gg 1$, the leading-order dispersion relation becomes

$$\Omega^2 \sim K(2m+n). \quad (2)$$

A similar closed-form analytical expression for waves in a magnetized polytrope, as of yet, is unknown. Earlier attempts (e.g., Gough & Thompson 1990; Spruit & Bogdan 1992; Cally & Bogdan 1993; Bogdan & Cally 1997;

Cally & Bogdan 1997) have ended with deriving, analytically, approximate integral expression in certain perturbative limits and then solving them numerically. Hence, they leave out the critical step of obtaining a straightforward analytical understanding of the effect of magnetic fields on linear asteroseismic waves. For example, Spruit & Bogdan (1992) consider a plane-parallel polytropic atmosphere threaded by a vertical magnetic field that is uniform throughout the whole domain. They perturbatively derive integrals for changes in wave frequency and then solve the integrals numerically. Cally & Bogdan (1993) pursue the model of Spruit & Bogdan (1992), but with a different perturbative approach. The effect of horizontal fields on waves is studied by several authors (e.g., Nye & Thomas 1976; Adam 1977; Thomas 1983; Campos 1983; Cally 2007; Campos & Marta 2015; Tripathi & Mitra 2022), but in simple and unrealistic isothermal atmosphere, which has very different properties of waves than in a more realistic polytropic atmosphere. Notably, Gough & Thompson (1990) treat a global problem (in spherical coordinates); there, the computation of eigenfrequencies requires evaluation of integral expressions using numerical methods [e.g., Eqs. (4.11)–(4.13) in Gough & Thompson (1990)]. A closed-form analytical formula is currently unavailable. The limitations of purely numerical approach and lack of a closed-form expression were succinctly expressed by Bogdan & Cally (1997):

“Ideally, we would wish to proceed by writing down an equation analogous to Lamb’s formula for the magnetized polytrope. Unfortunately, this approach is not feasible and for the most part one must instead be content with a numerically derived visual comparison of how the allowed oscillation frequencies depend upon the choice of the horizontal wavenumber k .”

Analytic dispersion relations are also essential for developing wave turbulence theory in the presence of both gravity and magnetic fields. In wave turbulence theory, calculations of mode resonances require simple, explicit dispersion relations that accurately capture the magnetic effect on observed linear waves. We note that the Lamb’s dispersion relation (2), $\Omega \sim \sqrt{K}$, is similar to that of surface gravity waves in oceans (Haselmann 1962). However, there is a critical difference: The surface gravity waves do not couple via three-wave resonance, thus requiring a weaker four-wave coupling (Nazarenko & Lukaschuk 2016). The Lamb waves, on the other hand, can couple via three-wave resonance, because there are infinitely many such waves (eigen-

states) at a given wavenumber, unlike only one pair of surface gravity waves at a given wavenumber. Thus, the infinitely many Lamb waves at a given wavenumber have distinct wave frequencies, which allow the sum of three frequencies at three wavenumbers to become null. While a wave turbulence theory for surface gravity waves has been well established, it is yet to be developed for the asteroseismic waves, whose dispersion relation in fully analytic form is a basic requirement for such a theory. The value that an analytic dispersion relation offers in resonant-coupling theory cannot be overstated when magnetic fields make the wave dispersion relation anisotropic and complicated. Motivated by these reasons, we seek here an accurate and simple formulae for the effect of magnetic fields on the Lamb waves.

Introducing magnetic fields, aligned orthogonal to a vertical gravity in Fig. 1, we find, as did Bogdan & Cally (1997), that the linearized magnetohydrodynamic (MHD) equations are too cumbersome to obtain a closed-form expression for the dispersion relation, even with the fast-wave approximation, $\Omega^2/K \gg 1$. Here, we overcome this difficulty by using both numerical simulations and extensive use of Mathematica, followed by a variant of the Jeffereys–Wentzel–Kramers–Brillouin (JWKB) approximation we devise to deduce

$$\Omega^2 \sim K(2m+n) \left[1 + \frac{\epsilon^2(4-2\gamma+\cos^2\theta-3\cos^4\theta)}{4} \right], \quad (3)$$

in the limit $\Omega^2/K \gg 1$, with $m = 0, 1, 2, \dots$. The parameter ϵ is the inverse of the Alfvénic Mach number, and θ is the angle the wave vector makes with the background magnetic field. Equation (3) is the principal result of this paper.

This paper is organized in the following way. In § 2, we describe our model and present the linearized compressible MHD equations. Such equations are then numerically solved in § 3. To obtain analytical understanding of the numerical results, the linearized equations are reduced to a wave equation in § 4. The normal-form wave equation is then perturbatively solved using a variant of the JWKB theory we construct; analytical understanding is gained in § 5. With astrophysical implications and roles of our results, we conclude in § 6.

2. SYSTEM SETUP AND LINEARIZED PERTURBATION EQUATIONS

To study waves in a magnetized, stratified medium, we consider the ideal three-dimensional compressible magnetohydrodynamic (MHD) equations (Chandrasekhar

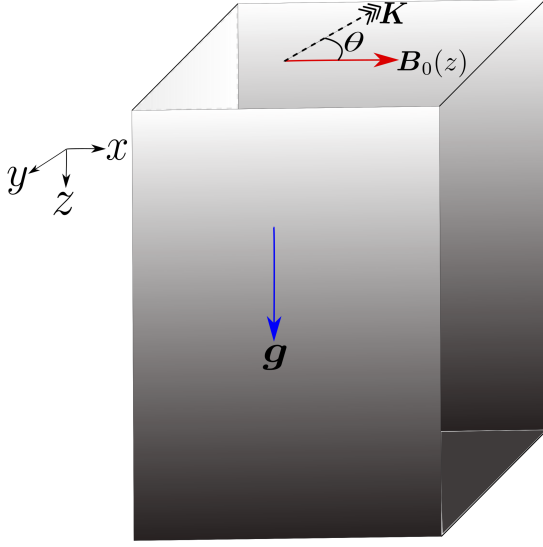


Figure 1. An inhomogeneous magnetic field $\mathbf{B}_0(z)$, oriented orthogonal to a constant vertical gravity \mathbf{g} , is considered where the wave is allowed to propagate in an arbitrary direction, shown with \mathbf{K} , making an angle θ with \mathbf{B}_0 . The gradient in the colormap of the box schematically represents increasing functions with depth z of the magnetic field, fluid density, pressure, and sound speed.

1961)

$$\partial_t \rho + \nabla \cdot (\rho \mathbf{U}) = 0, \quad (4a)$$

$$\rho [\partial_t \mathbf{U} + (\mathbf{U} \cdot \nabla) \mathbf{U}] = -\nabla P + \rho \mathbf{g} + \mathbf{J} \times \mathbf{B}, \quad (4b)$$

$$\partial_t \mathbf{B} = \nabla \times (\mathbf{U} \times \mathbf{B}), \quad (4c)$$

$$\frac{Dp}{Dt} = c^2 \frac{D\rho}{Dt}, \quad (4d)$$

where ρ , \mathbf{U} , P , and \mathbf{B} represent the density, the velocity, the pressure, and the magnetic field, respectively. The current density is $\mathbf{J} = \nabla \times \mathbf{B}/\mu_0$, where μ_0 represents the magnetic permeability of the vacuum. The magnetic field is additionally constrained to be divergence-less

$$\nabla \cdot \mathbf{B} = 0. \quad (5)$$

We consider a local Cartesian domain where the equilibrium density ρ_0 and pressure P_0 satisfy the polytropic relation

$$P_0 \sim \rho_0^{1+1/n}, \quad (6)$$

where n is the polytropic index of the gaseous atmosphere. In an unmagnetized atmosphere, the force balance gives $\partial_z P_0(z) = \rho_0(z)g$, where $\mathbf{g} = g\hat{\mathbf{e}}_z$, with g as the constant acceleration due to gravity along the vertical z -axis, as depicted in Fig. 1. The force balance requires

$$\rho_0(z) \sim z^n; \quad P_0(z) \sim z^{n+1}. \quad (7)$$

2.1. Background magnetic field and sound speed

We introduce an inhomogeneous background magnetic field, $\mathbf{B} = B_0(z)\hat{\mathbf{e}}_x$. The force-balance relation with the Lorentz force, $(\nabla \times \mathbf{B}/\mu_0) \times \mathbf{B}$, then becomes

$$\partial_z P_0 = \rho_0 g - \frac{1}{2\mu_0} \partial_z B_0^2. \quad (8)$$

The solution

$$B_0^2(z) \sim z^{n+1} \quad (9)$$

also satisfies Eq. (7). The plasma β is then a constant throughout the domain

$$\beta \equiv \frac{P_{\text{gas}}}{P_{\text{magnetic}}} = \frac{2\mu_0 P_0}{B_0^2}. \quad (10)$$

The sound speed (c) may now be deduced from Eq. (8), using $P_0 = c^2 \rho_0 / \gamma$, where γ is the adiabatic index of the gas

$$\partial_z c^2 = -\frac{nc^2}{z} + \frac{\gamma g}{1 + \beta^{-1}}. \quad (11)$$

The solution to Eq. (11) is $c^2 = c_0^2 z$, where c_0^2 is a constant given by

$$c_0^2 = \frac{\gamma g}{(n+1)(1 + \beta^{-1})}. \quad (12)$$

It is useful to express β^{-1} in terms of the Alfvénic Mach number M_A , which is the ratio of the the sound speed to the Alfvén speed,

$$\beta^{-1} = \frac{B_0^2}{\mu_0 \rho_0} \cdot \frac{\rho_0}{\gamma P_0} \cdot \frac{\gamma}{2} = \frac{\gamma}{2M_A^2}, \quad (13)$$

using which the sound speed becomes

$$c^2 = \frac{\gamma g z}{(n+1)(1 + \gamma M_A^{-2}/2)}. \quad (14)$$

2.2. Linearized perturbation equations

We now linearize the MHD equations around the background profiles $[\rho_0, \mathbf{0}, B_0, P_0]$, introduced in Eqs. (7) and (9). Such a linearization yields evolution equations for infinitesimal perturbations $[\tilde{\rho}, \tilde{\mathbf{u}}, \tilde{\mathbf{b}}, \tilde{p}]$ as

$$\partial_t \tilde{\rho} = -(\tilde{\mathbf{u}} \cdot \nabla) \rho_0 - \rho_0 (\nabla \cdot \tilde{\mathbf{u}}), \quad (15a)$$

$$\partial_t \tilde{u}_x = -\frac{\partial_x \tilde{p}}{\rho_0} + \frac{\tilde{b}_z \partial_z B_0}{\mu_0 \rho_0}, \quad (15b)$$

$$\partial_t \tilde{u}_y = -\frac{\partial_y \tilde{p}}{\rho_0} + \frac{B_0 (\partial_x \tilde{b}_y - \partial_y \tilde{b}_x)}{\mu_0 \rho_0}, \quad (15c)$$

$$\partial_t \tilde{u}_z = -\frac{\partial_z \tilde{p}}{\rho_0} + \frac{\tilde{\rho} g}{\rho_0} + \frac{B_0 (\partial_x \tilde{b}_z - \partial_z \tilde{b}_x) - \tilde{b}_x \partial_z B_0}{\mu_0 \rho_0}, \quad (15d)$$

$$\partial_t \tilde{b}_x = -B_0 (\partial_y \tilde{u}_y + \partial_z \tilde{u}_z) - \tilde{u}_z \partial_z B_0, \quad (15e)$$

$$\partial_t \tilde{b}_y = -B_0 \partial_x \tilde{u}_y, \quad (15f)$$

$$\partial_t \tilde{b}_z = -B_0 \partial_x \tilde{u}_z, \quad (15g)$$

$$\partial_t \tilde{p} = -(\tilde{\mathbf{u}} \cdot \nabla) P_0 - c^2 \rho_0 (\nabla \cdot \tilde{\mathbf{u}}). \quad (15h)$$

We shall use

$$\tilde{\chi} = \nabla \cdot \tilde{\mathbf{u}} \quad (16)$$

in the rest of the article, where helpful.

Equations (15a)–(15h) can be simplified to derive a set of fewer (closed) equations

$$\partial_t^2 \tilde{u}_x = c^2 \partial_x \tilde{\chi} + g \partial_x \tilde{u}_z, \quad (17a)$$

$$\partial_t^2 \tilde{u}_y = c^2 \partial_y \tilde{\chi} + g \partial_y \tilde{u}_z + \frac{c^2}{M_A^2} (\partial_{xx} \tilde{u}_y + \partial_y \tilde{\chi} - \partial_{xy} \tilde{u}_x), \quad (17b)$$

$$\begin{aligned} \partial_t^2 \tilde{u}_z = c^2 \partial_z \tilde{\chi} - g \partial_x \tilde{u}_x & \left[1 + \frac{\gamma}{M_A^2 (1 + \gamma M_A^{-2}/2)} \right] - g \partial_y \tilde{u}_y \\ & + \frac{\gamma (1 + M_A^{-2}) g \tilde{\chi}}{(1 + \gamma M_A^{-2}/2)} + \frac{c^2}{M_A^2} (\partial_{xx} \tilde{u}_z + \partial_z \tilde{\chi} - \partial_{xz} \tilde{u}_x). \end{aligned} \quad (17c)$$

We note that the appearance of M_A^2 in Eq. (17c) in certain terms may seem non-trivial at first sight; however, upon inspection, we understand them as terms emerging from the effect of the Lorentz force on the background states, via terms like $\partial_z c^2(z)$ and $(\partial_z P_0)/\rho_n$, while processing Eqs. (15a)–(15h). Admittedly, Eqs. (17a)–(17c) are somewhat challenging to proceed with clarity. Thus, we now non-dimensionalize the equations to make them reasonably transparent.

2.3. Non-dimensionalized linear equations

We define L as the characteristic length scale over which the sound speed varies (and, for that matter, pressure, density, and temperature also vary) appreciably. Then we find that the characteristic sound speed in an unmagnetized polytrope is, using Eq. (14), $c_L = \sqrt{\gamma g L / (n + 1)}$. Using L and L/c_L as the dimensional length and time units, we non-dimensionalize all variables henceforth, starting with the sound speed

$$C^2 = \frac{c^2}{c_L^2} = \frac{Z}{1 + \gamma M_A^{-2}/2}, \quad (18)$$

where the lowercase dimensional variables (c and z) are cast as uppercase non-dimensional variables (C and Z). Thus we replace all the dimensional variables in Eqs. (17a)–(17c) using

$$(x, y, z) = (LX, LY, LZ), \quad (19a)$$

$$c^2 = c_L^2 \frac{Z}{1 + \gamma M_A^{-2}/2}, \quad (19b)$$

$$\partial_t \equiv \frac{c_L}{L} \partial_T, \quad (19c)$$

where the uppercase characters X, Y , and T represent non-dimensional variables.

We analyze perturbations by Fourier-transforming in the (x, y) -plane, viz.,

$$\tilde{u}_x(Z) = \int dK_X dK_Y d\Omega \hat{u}_x \exp [i(K_X X + K_Y Y + \Omega T)], \quad (20)$$

where the uppercase characters represent non-dimensional quantities, e.g., $\mathbf{K} \equiv (K_X, K_Y)$ is the non-dimensional wavevector in the (x, y) -plane, and Ω is the nondimensional frequency. Fourier analyzing Eqs. (17a)–(17c) and representing M_A^{-1} by ϵ henceforth, we write

$$\left[\frac{-\Omega^2 (1 + \gamma \epsilon^2 / 2)}{i K_X Z} \right] \hat{u}_x + \left[\frac{-(n+1)(1 + \gamma \epsilon^2 / 2)}{\gamma Z} \right] \hat{u}_z = \hat{\chi}, \quad (21a)$$

$$\begin{aligned} [-i \epsilon^2 K_X] \hat{u}_x + \left[\frac{-\Omega^2 (1 + \gamma \epsilon^2 / 2)}{i K_Y Z} + \frac{\epsilon^2 K_X^2}{i K_Y} \right] \hat{u}_y \\ + \left[\frac{-(n+1)(1 + \gamma \epsilon^2 / 2)}{\gamma Z} \right] \hat{u}_z = \hat{\chi} (1 + \epsilon^2), \end{aligned} \quad (21b)$$

$$\begin{aligned} \left[i K_X \left\{ \frac{1 + \gamma \epsilon^2 / 2}{\gamma} + \epsilon^2 \left(1 + \frac{Z \partial_Z}{n+1} \right) \right\} \right] \hat{u}_x \\ + \left[\frac{i K_Y (1 + \gamma \epsilon^2 / 2)}{\gamma} \right] \hat{u}_y + \left[\frac{-\Omega^2 (1 + \gamma \epsilon^2 / 2) + \epsilon^2 Z K_X^2}{n+1} \right] \hat{u}_z \\ = \left(\hat{\chi} + \frac{Z \partial_Z \hat{\chi}}{n+1} \right) (1 + \epsilon^2). \end{aligned} \quad (21c)$$

Equations (21a)–(21c) are general, without any approximation, and host all three families of MHD waves: the fast and slow magnetoacoustic waves, and the Alfvén waves. The Alfvén wave dispersion relation is reproduced by substituting $K_Y = 0$ and $K_X = K$ in Eq. (21b), which renders it to: either $\hat{u}_y = 0$ (the trivial solution), or $\Omega^2 = \epsilon^2 K^2 Z / (1 + \gamma \epsilon^2)$. This is indeed the dispersion relation of the Alfvén waves, which is confirmed by writing $\Omega^2 = K^2 v_A^2$, where $v_A^2 = B_0^2 / (\mu_0 \rho_0)$ is the squared Alfvén speed. This squared Alfvén speed is determined from Eq. (13) to be $\gamma P_0 / (\rho_0 M_A^2)$. Recognizing that $\gamma P_0 / \rho_0$ is the squared sound speed, given in Eq. (18) [derived from Eq. (11)], the squared Alfvén speed is $v_A^2 = \epsilon^2 Z / (1 + \gamma \epsilon^2)$.

3. EXACT NUMERICAL SOLUTION

We obtain fully converged numerical solution to Eqs. (21a)–(21c) by employing the spectral ‘‘Dedalus’’ framework (Burns et al. 2020). Referring to the Dedalus methods paper (Burns et al. 2020) for more details, we briefly outline the numerical procedures employed in Dedalus for eigenvalue problems. At each horizontal wavenumber (K_X, K_Y) , the state variables—the three

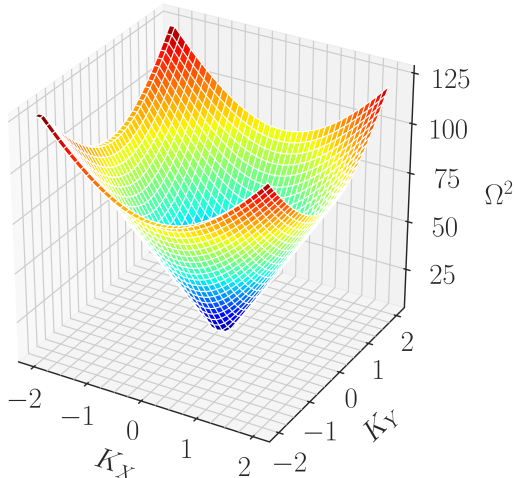


Figure 2. $\Omega^2(K_X, K_Y)$ for hydrodynamic and magnetized polytropes. The two plotted surfaces are visually indistinguishable because the difference ($\Delta\Omega^2$) between them is much smaller than Ω^2 ; see Fig. 3. The parameters used are $\epsilon = 0.1$, $m = 20$, $n = 2.5$, and $\gamma = 5/3$. For variations in these parameters, the surface plot of $\Omega^2(K_X, K_Y)$ remains the same qualitatively.

components of velocity—are expanded in the Chebyshev polynomials along the inhomogeneous z -axis. Because of the background inhomogeneity, different Chebyshev coefficients couple, creating a dense linear operator. Sparsification is provided by a change of basis from the Chebyshev polynomials of the first kind to those of the second kind. To impose boundary conditions and keep the matrix sparse, Dirichlet preconditioning is applied. Efficient solution of the resulting matrices is then found by passing the matrices \mathcal{L} and \mathcal{M} in the eigenvalue (σ) problem, $\mathcal{L}\mathcal{X} = \sigma\mathcal{M}\mathcal{X}$, to the “scipy” linear algebra packages. For a given spectral resolution along the inhomogeneous z -axis, we solve for all the eigenvalues of the matrices. Such a non-targeted, general solution produces a complete eigenspectrum and eigenmodes, corresponding to all families of linear MHD waves: the (fast) pressure-driven, (slow) gravity-driven modes, and the Alfvén modes. We focus on the high-frequency modes to assess the effect of magnetic fields on such fast pressure-driven waves.

For the boundary condition, at the lower boundary $z = L_z$, we require $\tilde{u}_z = 0$. At the upper boundary, $z = 0$, where the atmosphere ceases, we enforce, following Lamb (1911),

$$\frac{Dp}{Dt} = 0, \quad (22)$$

which implies

$$c^2 \frac{D\rho}{Dt} = -c^2 \rho_0 \tilde{\chi} = 0 = z^{n+1} \tilde{\chi}. \quad (23)$$

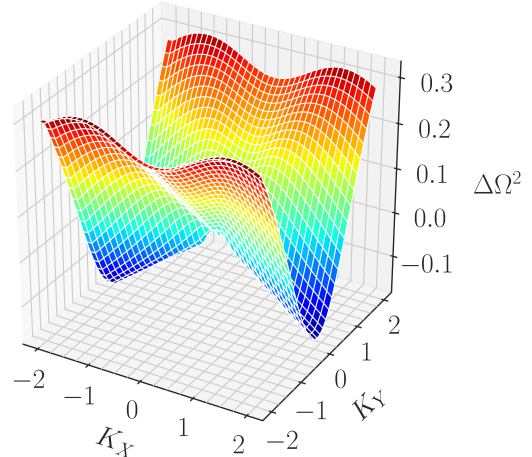


Figure 3. $\Delta\Omega^2 = \Omega^2 - \Omega_{\text{hydro}}^2$ is plotted for a magnetized polytrope, with $\epsilon = 0.1$, $m = 20$, $n = 2.5$, and $\gamma = 5/3$. This surface plot shows the difference between the two surface plots in Fig. 2.

We first validate that, in the absence of the magnetic field, our solver successfully reproduces two branches of Lamb’s exact analytical dispersion relation [Eq. (1)]. We identify the pressure-driven modes by comparing their eigenfrequencies with those predicted by Lamb’s solution. We then impose a very weak background magnetic field and systematically increase its strength, and track changes to the eigenfrequencies. A case of such magnetic modification of pressure-driven waves is shown in Fig. 2. Although, in Fig. 2, we display two surface plots of $\Omega^2(K_X, K_Y)$ —one for the hydrodynamic and other for the magnetized polytrope—the two plots are visually indistinguishable. The difference between the two surface plots is shown in Fig. 3. For $K_Y = 0$, $\Delta\Omega^2$ is negative, and for $K_X = 0$, $\Delta\Omega^2$ is positive and relatively large. We also note a minor decrease in positive value of $\Delta\Omega^2$ in going from $K_X \approx 0$ to $K_X = 0$.

It turns out that $\Delta\Omega^2$ is related to the hydrodynamic squared-frequency Ω_{hydro}^2 ; and $\Delta\Omega^2/\Omega_{\text{hydro}}^2$ is almost entirely independent of the wavevector magnitude (Fig. 4). Only angular dependence is observed.

The extremely low wavenumbers in Fig. 4 correspond to very large scale waves that cannot be captured in a finite box in numerical calculation. To capture lower wavenumbers, we significantly extend the domain size along the vertical z -axis, which allow us to obtain fully converged numerical results for other wavenumbers.

4. REDUCTION TO WAVE EQUATION

To analytically determine the dispersion relation, we solve the set of equations (21a)–(21c) perturbatively in the limit of a weak magnetic field, i.e., $\epsilon \ll 1$. By setting

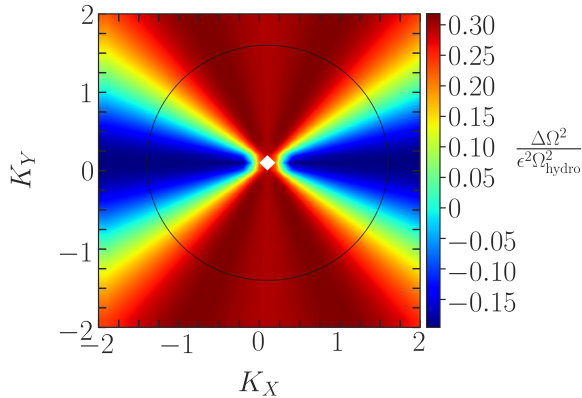


Figure 4. Relative difference of squared-frequency depends on the wavevector propagation angle (spanned by the black circle), but the relative difference is insensitive to the wavevector magnitude. The parameters chosen are $\epsilon = 0.1$, $m = 20$, $n = 2.5$, and $\gamma = 5/3$.

$\epsilon = 0$, we recover the Lamb’s equations for the unmagnetized polytrope (Lamb 1911). The Lamb’s equations reduce to a second-order differential equation for $\hat{\chi}$. With the same goal, we proceed in the following manner. We rewrite Eqs. (21a)–(21c) as

$$\begin{bmatrix} M_{11} & M_{12} & M_{13} \\ M_{21} & M_{22} & M_{23} \\ M_{31} & M_{32} & M_{33} \end{bmatrix} \begin{bmatrix} \hat{u}_x \\ \hat{u}_y \\ \hat{u}_z \end{bmatrix} = \begin{bmatrix} h_x(\hat{\chi}) \\ h_y(\hat{\chi}) \\ h_z(\hat{\chi}, \partial_Z \hat{\chi}) \end{bmatrix}, \quad (24)$$

where the matrix elements M_{ij} are independent of Z -derivatives, and are functions of $K_X, K_Y, \Omega, n, \gamma, \epsilon$, and Z only (for their complete expressions, see Appendix A). In arriving at Eq. (24), we have replaced $\partial_Z \hat{u}_x$ in the first term on the left-hand side of Eq. (21c) with its exact expression obtained by differentiating Eq. (21a) with respect to Z . We then substitute ∂_Z operation in $\partial_Z \hat{u}_z$ by writing it as $\hat{\chi} - iK_X \hat{u}_x - iK_Y \hat{u}_y$. Such a process removes ∂_Z operation from the matrix M . The functions h_ν are linear in $\hat{\chi}$ and $\partial_Z \hat{\chi}$.

Straightforward inversion of the matrix M expresses all components of the velocity in terms of $\hat{\chi}$ and $\partial_Z \hat{\chi}$:

$$\hat{u}_\nu = f_\nu(Z) \hat{\chi} + g_\nu(Z) \partial_Z \hat{\chi}, \quad (25)$$

where ν can be either x, y , or z . We recognize that f_ν and g_ν are functions of Z , but do not involve ∂_Z . The three velocity components of Eq. (25) can now be subsumed into a single second-order differential equation for $\hat{\chi}$:

$$\partial_Z^2 \hat{\chi} + P(Z, \epsilon) \partial_Z \hat{\chi} + R(Z, \epsilon) \hat{\chi} = 0, \quad (26)$$

which can be recast into the normal form of the second-order differential equation by changing variable as

$$\hat{\chi}(Z) = \hat{\psi}(Z) \exp \left[-\frac{1}{2} \int_Z dZ P(Z) \right], \quad (27)$$

which reduces Eq. (26) to the wave equation

$$\partial_Z^2 \hat{\psi} + \Gamma^2(Z, \epsilon, \delta) \hat{\psi} = 0. \quad (28)$$

In (28), we use the explicit notation $\Gamma^2(Z, \epsilon, \delta)$ to remind us that the two small parameters ϵ and δ are implicit in Γ , where $\delta = K/\Omega^2$, with $K = \sqrt{K_X^2 + K_Y^2}$ representing the magnitude of the wavevector and Ω representing the eigenfrequency.

The procedure outlined above appears straightforward. However, the analytical manipulations in arriving at Eq. (28)—a magnetized version of Lamb’s equation—require laborious and careful calculations, as $\Gamma^2(Z, \epsilon, \delta)$ alone conceals an expression of exhaustive length—tens of pages of this article. In the absence of the magnetic field, the expression for $\Gamma^2(Z, \epsilon = 0, \delta) = \Gamma_0^2(Z, \delta)$ is beautifully short, $\Gamma_0(Z, \delta) = K^2(Z - \alpha)(\beta - Z)/Z^2$, where α and β are the two turning points—two zeros of $\Gamma_0(Z, \delta)$ —that depend on δ , the property of the eigenfrequency.

5. PERTURBATIVE SOLUTION FOR ANISOTROPIC MAGNETIC EFFECT

The presence of a weak magnetic field, characterized by small ϵ , may be considered as a perturbation to the Lamb’s two-turning-point eigenvalue problem. Hence, the magnetic field changes both the locations of the turning points and the form of the potential $\Gamma(Z, \epsilon, \delta)$.

5.1. Perturbative calculations

A formal asymptotic solution to Eq. (28) is constructed by introducing a book-keeping, small parameter $^1 \zeta$ in (28) (see e.g., Bender & Orszag 1978; Tripathi 2022):

$$\zeta^2 \partial_Z^2 \hat{\psi} + \Gamma^2(Z, \epsilon, \delta) \hat{\psi} = 0. \quad (29)$$

To find the magnetically modified eigenfrequencies, we develop below an asymptotic theory starting from Eq. (29), by using perturbative expansions in powers of ζ, ϵ , and δ , in that order.

Following the standard procedure of the ζ -expansion of the state vector $\hat{\psi}$, we write the JWKB quantization condition (see e.g., Bender & Orszag 1978; Tripathi 2022),

$$\frac{1}{\pi} \int_{Z_1(\epsilon, \delta)}^{Z_2(\epsilon, \delta)} \Gamma(Z, \epsilon, \delta) dZ \sim \left(m + \frac{1}{2} \right); \quad m = 0, 1, 2, \dots, \quad (30)$$

where m refers to the eigenstate index, $\Gamma(Z, \epsilon, \delta)$ is the magnetically modified wavenumber, and $Z_1(\epsilon, \delta)$

¹ The parameter ζ can be replaced with unity at the outset or after performing the ζ -expansion.

and $Z_2(\epsilon, \delta)$ are the magnetically shifted turning points. Equation (30) is the leading-order contribution in the conventional JWKB asymptotic series, where the terms corresponding to the first two orders in ζ are retained. The first-order term yields $1/2$, shown on the right. Higher-order terms in ζ can be computed, see, e.g., Eqs. (7) to (10) of [Tripathi \(2022\)](#).

Next, we expand the wavenumber $\Gamma(Z, \epsilon, \delta)$ as

$$\Gamma(Z, \epsilon, \delta) = \Gamma_0(Z, \delta) + \epsilon \Gamma_1(Z, \delta) + \epsilon^2 \Gamma_2(Z, \delta) + \epsilon^3 \Gamma_3(Z, \delta) + \mathcal{O}(\epsilon^4). \quad (31)$$

Note that the leading-order effect of the Lorentz force on the wavefrequency appears only at the second order $\mathcal{O}(\epsilon^2)$ in the expansion, i.e., $\Gamma_1(Z, \delta)$ above is zero. The expressions for $\Gamma_0(Z, \delta)$ and $\Gamma_2(Z, \delta)$ are

$$\Gamma_0(Z, \delta) = \frac{K \sqrt{(Z - \alpha)(\beta - Z)}}{Z}, \quad (32a)$$

$$\Gamma_2(Z, \delta) = \frac{(b_2 Z^2 + b_1 Z + b_0)}{\sqrt{(Z - \alpha)(\beta - Z)}}, \quad (32b)$$

where we have used $K_X = K \cos \theta$ and $K_Y = K \sin \theta$. The parameters α and β depend on $\delta = K/\Omega^2$ and satisfy the following properties

$$\alpha\beta = \frac{n(n+2)}{4K^2}, \quad (33a)$$

$$\alpha + \beta = \left[\frac{\Omega^2}{K} - \frac{(n+1)(n+1-n\gamma)K}{\gamma^2} \right] \frac{1}{K}. \quad (33b)$$

The lengthy expressions of b_0 , b_1 , and b_2 are presented in Appendix B. We note that these parameters depend on Ω , K , θ , n , and γ only.

Now we expand the turning points $Z_1(\epsilon, \delta)$ and $Z_2(\epsilon, \delta)$ around the turning points of the unmagnetized polytrope, $Z_1^{(0)} = \alpha$ and $Z_2^{(0)} = \beta$ in powers of ϵ . For clarity we now suppress the implicit δ -dependence of the turning points. For example, we write $Z_j(\epsilon, \delta)$ as $Z_j(\epsilon)$, which we expand in powers of ϵ as

$$Z_j(\epsilon) = Z_j^{(0)} + \epsilon Z_j^{(1)} + \epsilon^2 Z_j^{(2)} + \mathcal{O}(\epsilon^3), \quad (34)$$

where $j = 1$ and $j = 2$ refer to the left and the right turning points, respectively (i.e., $\alpha < \beta$). We note that, in Eq. (34), the correction term at the first order in ϵ is zero, i.e., $Z_j^{(1)} = 0$. We find this result by substituting the expression for $Z_j(\epsilon)$ from Eq. (34) in $\Gamma(Z, \epsilon) = 0$, and by employing Eq. (31). Solving the resulting equation order-by-order in ϵ produces $Z_j^{(1)} = 0$. We note, however, that, at the second order in ϵ (which is where the effect of the Lorentz force comes in action), $Z_j^{(2)}$ becomes non-zero. The expressions for $Z_j^{(2)}$ are given in Appendix C.

Because the term $Z_j^{(2)}$ appears at the second order in ϵ , it may be tempting to assume that the term contributes to second order in ϵ itself in the JWKB integral in (30). This, however, is not the case. The term contributes to third and higher orders in ϵ as we show next. Expanding Eq. (30),

$$\frac{1}{\pi} \int_{Z_1^{(0)} + \epsilon^2 Z_1^{(2)} + \mathcal{O}(\epsilon^3)}^{Z_2^{(0)} + \epsilon^2 Z_2^{(2)} + \mathcal{O}(\epsilon^3)} [\Gamma_0(Z) + \epsilon^2 \Gamma_2(Z) + \mathcal{O}(\epsilon^3)] dZ \sim \left(m + \frac{1}{2} \right); \quad m = 0, 1, 2, \dots \quad (35)$$

We now integrate $\Gamma_0(Z)$ as

$$\begin{aligned} & \int_{Z_1^{(0)} + \epsilon^2 Z_1^{(2)} + \mathcal{O}(\epsilon^3)}^{Z_2^{(0)} + \epsilon^2 Z_2^{(2)} + \mathcal{O}(\epsilon^3)} \Gamma_0(Z) dZ \\ &= \left(\int_{\alpha + \epsilon^2 Z_1^{(2)} + \mathcal{O}(\epsilon^3)}^{\alpha} + \int_{\alpha}^{\beta} + \int_{\beta}^{\beta + \epsilon^2 Z_2^{(2)} + \mathcal{O}(\epsilon^3)} \right) \Gamma_0(Z) dZ \\ &= -\frac{2\epsilon^3 K(\beta - \alpha)^{1/2} [Z_1^{(2)}]^{3/2}}{3\alpha} + \int_{\alpha}^{\beta} \Gamma_0(Z) dZ \\ &\quad + \frac{2\epsilon^3 K(\beta - \alpha)^{1/2} [-Z_2^{(2)}]^{3/2}}{3\beta} + \mathcal{O}(\epsilon^4), \end{aligned} \quad (36)$$

where we notice terms with ϵ^3 arising from the second-order shifts in the turning points, $\epsilon^2 Z_1^{(2)}$ and $\epsilon^2 Z_2^{(2)}$. The additional power of ϵ emerges from the integrand $\Gamma_0(Z)$, which has a term $\sqrt{Z - Z_j^{(0)}}$. This term when expanded around $Z_j^{(0)}$ in powers of ϵ contributes an ϵ to the integral.

In Eq. (36), the term $\int_{\alpha}^{\beta} \Gamma_0(Z) dZ$ is the integral that one finds in Lamb's calculations. Since here we seek the effect of magnetic fields on Lamb waves, we replace $\int_{\alpha}^{\beta} \Gamma_0(Z) dZ$ with Lamb's exact dispersion relation for hydrodynamic waves [Eq. (1)]:

$$\begin{aligned} & \frac{1}{\pi} \int_{\alpha}^{\beta} \Gamma_0(Z) dZ \equiv \\ I_{\text{Lamb}} &= \frac{(n+1)}{2} \left[\frac{\Omega^2}{K(n+1)} + \frac{(\gamma n - n - 1)K}{\gamma^2 \Omega^2} - 1 \right] + 1. \end{aligned} \quad (37)$$

Thus, we replace the integral $\int_{\alpha}^{\beta} \Gamma_0(Z) dZ$, appearing in Eq. (36), with I_{Lamb} from Eq. (37) to obtain

$$\begin{aligned} I_{\text{Lamb}} &+ \frac{\epsilon^2}{\pi} \int_{\alpha}^{\beta} \Gamma_2(Z) dZ + \mathcal{O}(\epsilon^3) \\ &\sim \left(m + \frac{1}{2} \right); \quad m = 0, 1, 2, \dots, \end{aligned} \quad (38)$$

which is accurate up to second order in ϵ . We substitute $\Gamma_2(Z)$ from Eq. (32b) and perform the integral in

Eq. (38) to arrive at

$$I_{\text{Lamb}} - \epsilon^2 \left[b_0 + b_1 \left(\frac{\alpha + \beta}{2} \right) + b_2 \left(\frac{3\alpha^2 + 2\alpha\beta + 3\beta^2}{8} \right) \right] \sim \left(m + \frac{1}{2} \right); \quad m = 0, 1, 2, \dots \quad (39)$$

Employing fast-wave approximation, we now expand each term on the left-hand side of Eq. (39) in powers of $\delta = K/\Omega^2$ as

$$I_{\text{Lamb}} \approx \frac{1}{\delta} \left[\frac{1}{2} + \frac{\delta(1-n)}{2} + \mathcal{O}(\delta^2) \right], \quad (40a)$$

$$b_0 \approx \frac{1}{\delta} \left[\frac{2-\gamma}{4} + \mathcal{O}(\delta^2) \right], \quad (40b)$$

$$b_1 \left(\frac{\alpha + \beta}{2} \right) \approx \frac{1}{\delta} \left[\frac{\cos^2 \theta}{4} + \mathcal{O}(\delta^2) \right], \quad (40c)$$

$$b_2 \left(\frac{3\alpha^2 + 2\alpha\beta + 3\beta^2}{8} \right) \approx \frac{1}{\delta} \left[\frac{-3 \cos^4 \theta}{8} + \mathcal{O}(\delta^2) \right]. \quad (40d)$$

Thus we obtain a simplified dispersion relation from Eq. (39):

$$\frac{\Omega^2}{K} \left[\frac{1}{2} - \frac{\epsilon^2}{4} \left\{ 2 - \gamma + \cos^2 \theta - \frac{3 \cos^4 \theta}{2} \right\} \right] \sim \left(m + \frac{n}{2} \right); \quad m = 0, 1, 2, \dots \quad (41)$$

It turns out that Eq. (41) does not agree excellently with our numerical results, see Fig. A1 in Appendix D. But replacing $\cos^2 \theta$ with $(\cos^2 \theta)/2$ gives excellent agreement.

Informed in this way, we write the final dispersion relation

$$\boxed{\frac{\Omega^2}{K} \left[\frac{1}{2} - \frac{\epsilon^2}{4} \left\{ 2 - \gamma + \frac{\cos^2 \theta}{2} - \frac{3 \cos^4 \theta}{2} \right\} \right] \sim \left(m + \frac{n}{2} \right); \quad m = 0, 1, 2, \dots} \quad (42)$$

5.2. Comparison between theory and numerics

Using the Lamb's relation, $\Omega_{\text{hydro}}^2 \sim K(2m+n)$, we rewrite Eq. (42) as

$$g(\theta) \equiv \gamma/2 + \Delta\Omega^2/(\epsilon^2\Omega_{\text{hydro}}^2) = 1 + \frac{1}{4} (\cos^2 \theta - 3 \cos^4 \theta), \quad (43)$$

where $\Delta\Omega^2 \equiv \Omega^2 - \Omega_{\text{hydro}}^2$. This is a remarkable result. The right-hand-side of Eq. (43) is independent of every other possible parameter other than θ ! In Fig. 5, we plot the function $g(\theta)$ from our numerical determination of

the eigenfrequencies for numerous different values of m and K , and two different values of ϵ , and two different values of γ . These numerical values are shown with different markers. All the different curves collapse onto each other, creating a universal master curve. We also plot our asymptotic expression, Eq. (42), which agrees very well with the numerical results. This demonstrates that our theory is in excellent agreement with numerics even for ϵ as large as $\epsilon = 0.1$.

It is surprising that, in our attempt to capture the anisotropy brought in by the magnetic field, despite a myriad of unwieldy expressions encountered on the way, an expression as simple as Eq. (42), is obtained. This simple expression is also highly accurate, as demonstrated in Fig. 5. The gratifying success of our asymptotic theory is somewhat unexpected, given that the analytical solution is accurate only up to the leading order in ζ, ϵ , and $\delta = K/\Omega^2$.

More accurate solutions may be obtained by using the full expressions of b_0, b_1 , and b_2 from Appendix B in Eqs. (40d)–(40b), and retaining higher-order terms in ζ and ϵ .

We emphasize that the closed-form expression we obtain is not solely by use of the perturbative calculation. At the last step, we needed guidance from our numerical solutions. This implies that future work should develop a better perturbation theory. We discuss a few possibilities. Let us first revisit our perturbative calculation. Equation (28) is exact. It has two small parameters, ϵ and δ . For $\epsilon = 0$, this equation reduces to the Lamb's problem. We note that our final dispersion relation (42) reproduces the high-frequency Lamb's dispersion relation (2) if we set $\epsilon = 0$ in Eq. (42). In our perturbative calculation, we also introduce the additional small parameter ζ to allow us to use the JWKB formalism. The first step then is to retain the first two leading-order terms in ζ . Thus we obtain Eq. (30). We arrive at a curious JWKB problem where the turning points themselves depend on a small parameter ϵ , see Eq. (35). We retain terms up to second order in ϵ in this expansion, thereby arriving at Eq. (38). Next, we expand all terms in powers of δ . If we change the order of expansion in ϵ and δ , then we no longer obtain the mathematical structure of the two-turning-point JWKB problem. The leading-order term reduces to an expression whose Z -dependence is solely $Z^{-1/2}$. To reformulate that expansion such that we can compare it with the Lamb's result, we must resum the δ -expanded infinite series which is not straightforward. So, this does not seem to be a useful alternative. Next, we remind the reader that a naive application of the JWKB method to calculate eigenvalues of the Schrodinger equation for either the harmonic

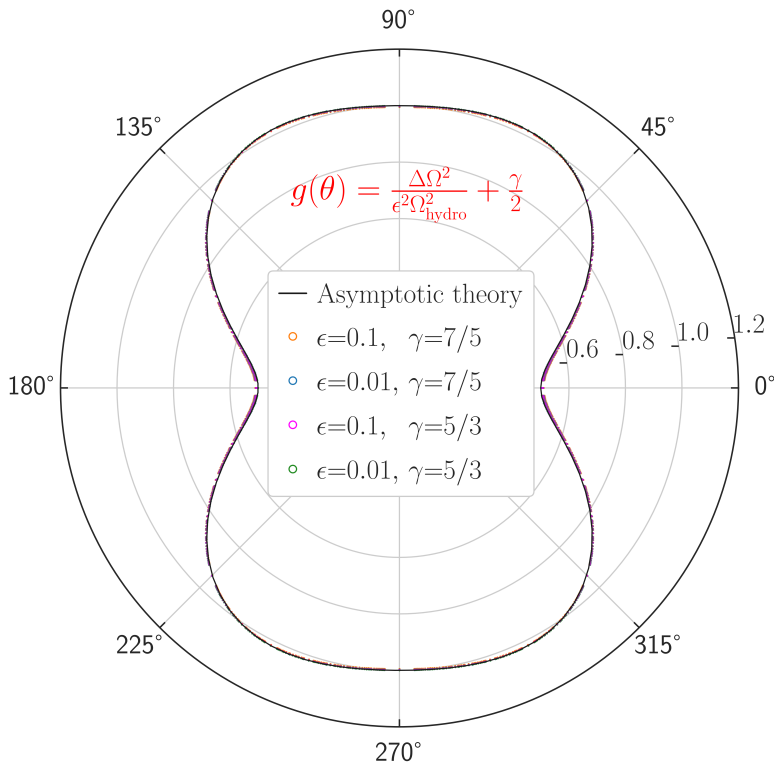


Figure 5. Theory and numerics: Our theory predicts that $g(\theta) = \Delta\Omega^2/(\epsilon^2\Omega_{\text{hydro}}^2) + \gamma/2$ depends only on θ as given in Eq. (43). The function $g(\theta)$ is independent of the wavenumber K , Alfvénic Mach number ϵ^{-1} , the polytropic index n , the adiabatic index γ , and the eigenstate index m . Here, we plot $g(\theta)$ obtained from our numerical solutions for several different values of m , ranging from 10 to 35, and for several different values of K ($0.6 \leq |K| \leq 2$), and for two values of ϵ and two values of γ (different symbols). All data points collapse on the same universal curve. The function $g(\theta)$ from our asymptotic theory, Eq. (43), is also plotted here. The asymptotic curve is indistinguishable from the exact numerical solutions.

oscillator or the Coulomb potential in three dimensions gives a factor of $\ell(\ell+1)$ [ℓ is the quantum number for orbital angular momentum], which must be replaced with $(\ell+1/2)^2$ to obtain the correct expression (Langer 1937). This correction appears naturally when the JWKB series is resummed to all orders (Romanovski & Robnik 2000; Robnik & Salasnich 1997; Tripathi 2022). Hence, there is a possibility that a resummation of the higher-order terms in powers of ζ may reproduce Eq. (42). Finally, we note the third possibility. We mapped Eq. (26) to a form amenable to the JWKB method. Instead, for $\epsilon = 0$, Eq. (26) can be transformed to the confluent hypergeometric equation—this is how Lamb first solved for the waves in a hydrodynamic polytrope. Thus, for a small ϵ , it is possible to use the method of multiple scales in a way such that the confluent hypergeometric functions appear as leading-order solutions, allowing to compute perturbed eigenfrequencies.

5.3. Role in helioseismic inversions

Since our theoretical formula and numerics show in Fig. 5 that the expression $\Delta\Omega^2/(\epsilon^2\Omega_{\text{hydro}}^2) + \gamma/2$ collapses on a single universal curve $g(\theta) = 1 +$

$\frac{1}{4}(\cos^2\theta - 3\cos^4\theta)$, it suggests that high-frequency helioseismic oscillation data should collapse on a single curve if one plots the fractional change in observed frequency compared to the Lamb’s hydrodynamic model. Such a plot allows extraction of two parameters: ϵ^2 , which encodes the magnetic field strength, and γ , which is the adiabatic index of the gaseous atmosphere. Since our theory is applicable to high-frequency ($m \gg 1$) waves, the polytropic index n cannot be inferred reliably using our method, as the squared-frequency of oscillations in the hydrodynamic model in Eq. (2) scales as $2m + n \sim 2m$.

We also note that we have considered a horizontal magnetic field in local Cartesian coordinates, which corresponds to non-radial magnetic fields in spherical coordinates. Such non-radial fields are found to be the most sensitive to the helioseismic inversion kernels near the solar surface (Das 2022; Das et al. 2020). This justifies our consideration. Note further that the inversion kernels in general are model-dependent, and the models for stars other than the Sun are not well-constrained. Since our formula has only two fitting parameters, more reliable estimation of those parameters is possible.

The effect of magnetic fields on slow gravity-driven waves is not considered in this paper, as the gravity-driven waves generally penetrate deep in the core of a star, which requires global geometry. Our current analysis in the Cartesian domain is appropriate for the fast pressure-driven waves that are confined in the sub-surface layers of a star. We shall nevertheless remark briefly on the potential impact of magnetic fields on slow gravity-driven waves. For the slow waves, the first term on the left-hand side of Eq. (1) may be neglected, which implies: (i) squared time period of such waves is linearly proportional to the eigenstate index, and (ii) such waves in unmagnetized medium become unstable when $\gamma < (1 + 1/n)$. This instability criterion (ii) is consistent with the energy principle of Newcomb (1961). When a magnetic field is present, by applying the energy principle of Newcomb, we find, for $K_X \neq 0$,² the instability threshold on γ for the gravity waves is lifted to $\gamma < (1 + 1/n)(1 + 1/\beta)$. When the magnetic field is very strong ($\beta \ll 1$), the regular perturbation series in powers of ϵ ($\propto 1/\sqrt{\beta}$) is possibly inadequate for unstable gravity-driven waves. Such considerations are clearly beyond the scope of the present paper. We note, however, that thorough understanding of the effect of magnetic fields on mixed gravito-acoustic waves holds a promise to deliver reliable estimation of the strengths and geometries of magnetic fields that are buried in deep layers of stellar interiors (Bugnet et al. 2021; Mathis et al. 2021; Mathis & Bugnet 2023). As a testament to this promise, recent global asteroseismic studies have detected and characterized magnetic fields in the core of red giant stars, opening a wholly new avenue to magnetoseismology (Li et al. 2022, 2023; Deheuvels et al. 2023).

6. CONCLUSIONS

Here we derive, for pressure-driven waves, an accurate and simple analytical formula that captures the effects of magnetic field and five other parameters: adiabatic index, polytropic index, eigenmode state index, wavenumbers, and the angle between the wavevector and the magnetic field [$\theta = \cos^{-1}(\hat{\mathbf{K}} \cdot \hat{\mathbf{B}}_0)$]. Such a six-parameter-dependent formula is distilled using a perturbative solution to magnetized version of Lamb's hydrodynamic polytropic waves. Our explicit analytical formula overcomes the limitation of previously attempted formulae for the magnetized polytrope that were presented in general integral forms; such a formulation, for instance, that of Gough & Thompson [1990; e.g., Eq. (4.11)] and Bog-

dan & Cally (1997), requires numerical evaluation of the eigenfrequencies, and thus leaves out the critical step of obtaining an analytical understanding and expression. We arrive at our result, guided by our numerical solutions and at the cost of extensive use of Mathematica for our perturbative analyses.

The simplicity and accuracy of our formula are encouraging to employ the formula to help solve the inverse problem of magnetoseismology. Our formula provides an explicit, analytical dependence of the observed surface oscillation frequency with the orientation and strength of the subsurface magnetic field. Such an understanding may be able to predict the surface-emergence location and strength of active regions, and to understand the properties of subsurface dynamo, e.g., magnetic activity in the near-surface shear layer (Vasil et al. 2024).

Nonlinear asteroseismology can also directly benefit from our analytical work, as weak turbulence theory of asteroseismic waves inevitably requires accurate and simple expressions of linear wave frequencies in resonant triad interactions. The effect of the magnetic field on such waves remains unknown. However, observations now exist that suggest resonant mode interactions are possible and can be a critical element of strongly pulsating stars (Guo 2020). Nonlinear mode coupling of linear eigenmodes (Tripathi et al. 2023a,b; Tripathi et al. 2024) may also need to be analyzed, in addition to mode resonances. Future planned research will directly take advantage of the formula derived here to assess the role of the magnetic field and other parameters in asteroseismic wave turbulence, which is eagerly awaiting to soon enter adulthood from its infancy.

ACKNOWLEDGMENTS

We are pleased to thank Ellen G. Zweibel for helpful discussions and for her contribution in applying the energy principle of Newcomb (1961) to our system. We are grateful to Srijan B. Das and the anonymous reviewer for their feedback that improved the paper. The inception of this paper took place at Nordic Institute for Theoretical Physics (NORDITA), Sweden, while B.T. was visiting on a research fellowship generously made available by NORDITA.

DATA AVAILABILITY

Mathematica notebook and Dedalus script used in this paper are deposited in <https://github.com/BindeshTripathi/polytrope>. The notebook is developed to perform lengthy analytical manipulations, and the python script is created for spectral numerical solution of linear MHD waves.

² For $K_X = 0$, the criterion for the gravity waves to become unstable is slightly modified: $\gamma < (1 + 1/n)(1 + 1/\beta) - 2/\beta$.

APPENDIX A

The matrix elements M_{ij} and h_μ that appear in Eq. (24) are

$$M_{11} = -\Omega^2(1 + \gamma\epsilon^2/2), \quad (\text{A1a})$$

$$M_{12} = 0, \quad (\text{A1b})$$

$$M_{13} = \frac{-iK_X(n+1)(1 + \gamma\epsilon^2/2)}{\gamma}, \quad (\text{A1c})$$

$$M_{21} = \epsilon^2 K_X K_Y Z, \quad (\text{A1d})$$

$$M_{22} = -\Omega^2(1 + \gamma\epsilon^2/2) + \epsilon^2 K_X^2 Z, \quad (\text{A1e})$$

$$M_{23} = \frac{-iK_Y(n+1)(1 + \gamma\epsilon^2/2)}{\gamma}, \quad (\text{A1f})$$

$$M_{31} = \frac{iK_X}{\gamma} \left[1 + \epsilon^2 \left(\frac{3\gamma}{2} + \frac{K_X^2 Z}{\Omega^2} \right) \right], \quad (\text{A1g})$$

$$M_{32} = \frac{iK_Y}{\gamma} \left[1 + \epsilon^2 \left(\frac{\gamma}{2} + \frac{K_X^2 Z}{\Omega^2} \right) \right], \quad (\text{A1h})$$

$$M_{33} = \frac{-\Omega^2(1 + \gamma\epsilon^2/2) + \epsilon^2 K_X^2 Z}{n+1}, \quad (\text{A1i})$$

$$h_x = iK_X Z \hat{\chi}, \quad (\text{A1j})$$

$$h_y = iK_Y Z \hat{\chi}(1 + \epsilon^2), \quad (\text{A1k})$$

$$h_z = \hat{\chi} + \frac{Z\partial_Z \hat{\chi}}{n+1} + \epsilon^2 \hat{\chi} \left[1 + \frac{K_X^2 Z \{ \gamma - (n+1)(1 + \gamma\epsilon^2/2) \}}{(n+1)\gamma\Omega^2(1 + \gamma\epsilon^2/2)} \right] + \epsilon^2 \frac{Z\partial_Z \hat{\chi}}{n+1} \left[1 + \frac{K_X^2 Z}{\Omega^2(1 + \gamma\epsilon^2/2)} \right]. \quad (\text{A1l})$$

APPENDIX B

The parameters introduced in Eq. (32b), while writing the expression for $\Gamma_2(Z)$, appear below:

$$b_2 = \frac{-K^3 \cos^4 \theta}{\Omega^2}, \quad (\text{A2a})$$

$$b_1 = \frac{-K \left[-\Omega^8 \gamma^4 + \Omega^4 \gamma^2 K^2 (n+1) \{ (n+1 + \gamma - \gamma n) \cos(2\theta) - n - 1 - 3\gamma \} + 2K^4 (n+1)^4 - K^4 (n+1)^3 (n+1 - \gamma n) \cos(2\theta) \right]}{2\Omega^4 \gamma^2 \sec^2 \theta \left[\Omega^4 \gamma^2 - K^2 (n+1)^2 \right]}, \quad (\text{A2b})$$

$$b_0 = \frac{\left(4\Omega^8 \gamma^4 (2 - \gamma) - 2\Omega^4 \gamma^2 K^2 \{ 2(n+1)^2 (4 - 3\gamma) + n(2n+3)\gamma^2 \} + K^4 (n+1)^2 \{ n\gamma^2 (2n+3) - 8(n+1)^2 (\gamma - 1) \} \right)}{16\Omega^2 \gamma^2 K \left[\Omega^4 \gamma^2 - K^2 (n+1)^2 \right]} \left[2K^2 \gamma \cos(2\theta) \left[K^2 (n+1)^2 \{ n(\gamma - 4 + 2n(\gamma - 1)) - 2 \} + \Omega^4 \gamma^2 \{ 2(n+1)^2 - \gamma n(2n+3) \} \right] + n\gamma^2 K^4 (n+1)^2 \cos(4\theta) \right] \quad (\text{A2c})$$

APPENDIX C

Due to the magnetic field, the locations of the turning points, Z_1 and Z_2 , shift—which to the second order in

ϵ in Eq. (34) are given by $Z_1^{(2)}$ and $Z_2^{(2)}$:

$$Z_1^{(2)} = \frac{\alpha(b_2 \alpha^2 + b_1 \alpha + b_0)}{K(\beta - \alpha)}, \quad (\text{A3a})$$

$$Z_2^{(2)} = \frac{-\beta(b_2 \beta^2 + b_1 \beta + b_0)}{K(\beta - \alpha)}. \quad (\text{A3b})$$

APPENDIX D

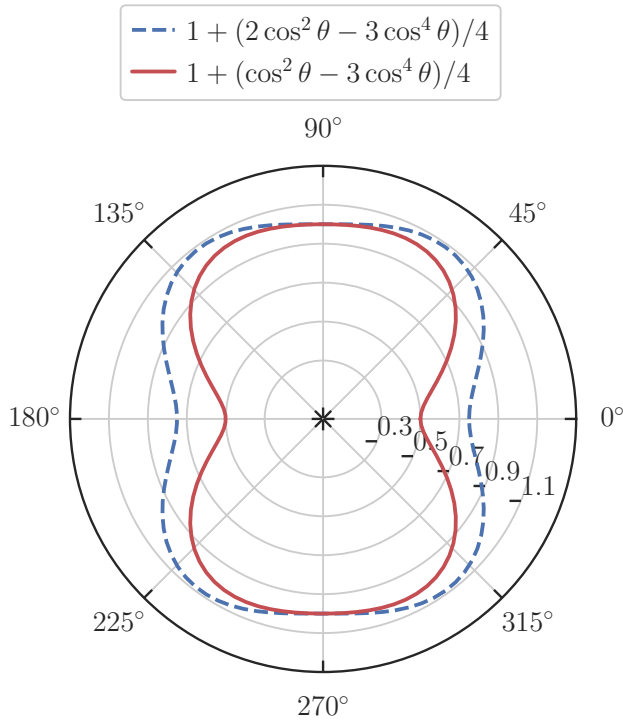


Figure A1. Comparison of different expressions to assess their individual contribution. The innermost (red) curve is the universal curve on which all numerical data collapse.

REFERENCES

- Adam, J. 1977, *Solar Physics*, 52, 293
- Aerts, C., Christensen-Dalsgaard, J., & Kurtz, D. W. 2010, *Asteroseismology* (Springer Science & Business Media)
- Bender, C. M., & Orszag, S. A. 1978, *Advanced Mathematical Methods for Scientists and Engineers*
- Bogdan, T. J., & Cally, P. S. 1997, *Proceedings of the Royal Society of London Series A*, 453, 943, doi: [10.1098/rspa.1997.0052](https://doi.org/10.1098/rspa.1997.0052)
- Bugnet, L., Prat, V., Mathis, S., et al. 2021, *A&A*, 650, A53, doi: [10.1051/0004-6361/202039159](https://doi.org/10.1051/0004-6361/202039159)
- Burns, K. J., Vasil, G. M., Oishi, J. S., Lecoanet, D., & Brown, B. P. 2020, *Physical Review Research*, 2, 023068, doi: [10.1103/PhysRevResearch.2.023068](https://doi.org/10.1103/PhysRevResearch.2.023068)
- Cally, P. S. 2007, *Astronomische Nachrichten*, 328, 286, doi: [10.1002/asna.200610731](https://doi.org/10.1002/asna.200610731)
- Cally, P. S., & Bogdan, T. 1997, *The Astrophysical Journal*, 486, L67
- Cally, P. S., & Bogdan, T. J. 1993, *ApJ*, 402, 721, doi: [10.1086/172172](https://doi.org/10.1086/172172)
- Campos, L. 1983, *Wave Motion*, 5, 1
- Campos, L., & Marta, A. 2015, *Geophysical & Astrophysical Fluid Dynamics*, 109, 168
- Chandrasekhar, S. 1961, *Hydrodynamic and hydromagnetic stability*, 652 pp., clarendon, Oxford, UK
- Das, S. B. 2022, *The Astrophysical Journal*, 940, 92
- Das, S. B., Chakraborty, T., Hanasoge, S. M., & Tromp, J. 2020, *The Astrophysical Journal*, 897, 38
- Deheuvels, S., Li, G., Ballot, J., & Lignières, F. 2023, *A&A*, 670, L16, doi: [10.1051/0004-6361/202245282](https://doi.org/10.1051/0004-6361/202245282)
- Gough, D., & Thompson, M. 1990, *Monthly Notices of the Royal Astronomical Society*, 242, 25
- Guo, Z. 2020, *ApJ*, 896, 161, doi: [10.3847/1538-4357/ab911f](https://doi.org/10.3847/1538-4357/ab911f)
- Hasselmann, K. 1962, *Journal of Fluid Mechanics*, 12, 481, doi: [10.1017/S0022112062000373](https://doi.org/10.1017/S0022112062000373)
- Iliadis, S., Zhao, J., & Kosovichev, A. 2011, *Science*, 333, 993, doi: [10.1126/science.1206253](https://doi.org/10.1126/science.1206253)
- Lamb, H. 1911, *Proceedings of the Royal Society of London Series A*, 84, 551, doi: [10.1098/rspa.1911.0008](https://doi.org/10.1098/rspa.1911.0008)
- Langer, R. E. 1937, *Physical Review*, 51, 669
- Li, G., Deheuvels, S., Ballot, J., & Lignières, F. 2022, *Nature*, 610, 43, doi: [10.1038/s41586-022-05176-0](https://doi.org/10.1038/s41586-022-05176-0)
- Li, G., Deheuvels, S., Li, T., Ballot, J., & Lignières, F. 2023, *A&A*, 680, A26, doi: [10.1051/0004-6361/202347260](https://doi.org/10.1051/0004-6361/202347260)

- Mathis, S., & Bugnet, L. 2023, *A&A*, 676, L9,
doi: [10.1051/0004-6361/202346832](https://doi.org/10.1051/0004-6361/202346832)
- Mathis, S., Bugnet, L., Prat, V., et al. 2021, *A&A*, 647, A122, doi: [10.1051/0004-6361/202039180](https://doi.org/10.1051/0004-6361/202039180)
- Nazarenko, S., & Lukaschuk, S. 2016, *Annual Review of Condensed Matter Physics*, 7, 61,
doi: [10.1146/annurev-conmatphys-071715-102737](https://doi.org/10.1146/annurev-conmatphys-071715-102737)
- Newcomb, W. A. 1961, *Physics of Fluids*, 4, 391,
doi: [10.1063/1.1706342](https://doi.org/10.1063/1.1706342)
- Nye, A. H., & Thomas, J. H. 1976, *ApJ*, 204, 573,
doi: [10.1086/154205](https://doi.org/10.1086/154205)
- Robnik, M., & Salasnich, L. 1997, *Journal of Physics A: Mathematical and General*, 30, 1711,
doi: [10.1088/0305-4470/30/5/031](https://doi.org/10.1088/0305-4470/30/5/031)
- Romanovski, V. G., & Robnik, M. 2000, *Journal of Physics A: Mathematical and General*, 33, 8549,
doi: [10.1088/0305-4470/33/47/315](https://doi.org/10.1088/0305-4470/33/47/315)
- Schunker, H., Braun, D. C., Cally, P. S., & Lindsey, C. 2005, *The Astrophysical Journal*, 621, L149
- Singh, N. K., Brandenburg, A., Chitre, S., & Rheinhardt, M. 2015, *Monthly Notices of the Royal Astronomical Society*, 447, 3708
- Singh, N. K., Brandenburg, A., & Rheinhardt, M. 2014, *The Astrophysical Journal Letters*, 795, L8
- Singh, N. K., Raichur, H., & Brandenburg, A. 2016, *The Astrophysical Journal*, 832, 120
- Singh, N. K., Raichur, H., Käpylä, M. J., et al. 2020, *Geophysical & Astrophysical Fluid Dynamics*, 114, 196
- Spruit, H. C., & Bogdan, T. J. 1992, *ApJL*, 391, L109,
doi: [10.1086/186409](https://doi.org/10.1086/186409)
- Thomas, J. H. 1983, *Annual Review of Fluid Mechanics*, 15, 321
- Tripathi, B. 2022, *PhRvD*, 105, 036010,
doi: [10.1103/PhysRevD.105.036010](https://doi.org/10.1103/PhysRevD.105.036010)
- Tripathi, B., Barker, A. J., Fraser, A. E., Terry, P. W., & Zweibel, E. G. 2024, *The Astrophysical Journal*, 966, 195, doi: [10.3847/1538-4357/ad38c3](https://doi.org/10.3847/1538-4357/ad38c3)
- Tripathi, B., Fraser, A. E., Terry, P. W., et al. 2023a, *Physics of Plasmas*, 30, 072107, doi: [10.1063/5.0156560](https://doi.org/10.1063/5.0156560)
- Tripathi, B., & Mitra, D. 2022, *ApJ*, 934, 61,
doi: [10.3847/1538-4357/ac79b1](https://doi.org/10.3847/1538-4357/ac79b1)
- Tripathi, B., Terry, P. W., Fraser, A. E., Zweibel, E. G., & Pueschel, M. J. 2023b, *Physics of Fluids*, 35, 105151,
doi: [10.1063/5.0167092](https://doi.org/10.1063/5.0167092)
- Van Beeck, J., Bowman, D. M., Pedersen, M. G., et al. 2021, *A&A*, 655, A59, doi: [10.1051/0004-6361/202141572](https://doi.org/10.1051/0004-6361/202141572)
- Van Beeck, J., Van Hoolst, T., Aerts, C., & Fuller, J. 2023, *arXiv e-prints*, arXiv:2311.02972,
doi: [10.48550/arXiv.2311.02972](https://doi.org/10.48550/arXiv.2311.02972)
- Vasil, G. M., Lecoanet, D., Augustson, K., et al. 2024, *Nature*, 629, 769, doi: [10.1038/s41586-024-07315-1](https://doi.org/10.1038/s41586-024-07315-1)